Derivation of gravity anomalies from Airborne Gravimeter, IMU recordings - validation with regional analytic models using ground and satellite gravity data

Jürgen Neumeyer, Uwe Schäfer, Jens Kremer Hartmut Pflug, Guochang Xu

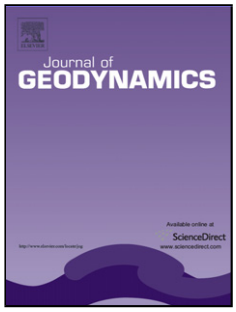

Title: Derivation of gravity anomalies from Airborne Gravimeter, IMU recordings - validation with regional analytic models using ground and satellite gravity data

Authors: Jürgen Neumeyer, Uwe Schäfer, Jens Kremer
Hartmut Pflug, Guochang Xu

PII: S0264-3707(08)00067-7
DOI: doi:10.1016/j.jog.2008.08.001
Reference: GEOD 864

To appear in: *Journal of Geodynamics*

Received date: 31-3-2008
Revised date: 1-8-2008
Accepted date: 21-8-2008

Please cite this article as: Neumeyer, J., Schäfer, U., Pflug, J.K.H., Xu, G., Derivation of gravity anomalies from Airborne Gravimeter, IMU recordings - validation with regional analytic models using ground and satellite gravity data, *Journal of Geodynamics* (2007), doi:10.1016/j.jog.2008.08.001

Derivation of gravity anomalies from Airborne Gravimeter and IMU recordings - validation with regional analytic models using ground and satellite gravity data

Jürgen Neumeyer[1,*], Uwe Schäfer[2], Jens Kremer[3] Hartmut Pflug[1], Guochang Xu[1]

[1)] Dept. of Geodesy & Remote Sensing, GeoForschungsZentrum Potsdam, Telegrafenberg A17, D-14473 Potsdam, Germany

[2)] Dept. of Geodesy, Bundesamt für Kartographie und Geodäsie, Karl-Rothe-Str. 10-14, D-04105 Leipzig, Germany

[3)] Ingenieur-Gesellschaft für Interfaces mbH, Langenauer Str. 46, D-57223 Kreuztal, Germany

*) Corresponding author, E-mail: Juergen_Neumy@yahoo.de

Abstract

For testing the performance of the upgraded LaCoste and Romberg airborne gravimeter S124 and evaluating the newly updated software, an airborne gravity test campaign has been carried out in the northern part of Germany by GFZ Potsdam in autumn 2006 using the aircraft Cessna 404 of "Hansa Luftbild" Company, Münster.

We present the results of a profile flown SW-NE in both directions at a nearly constant mean altitude of ~1100 m with a ground speed of ~230 km/h, crossing one of the most pronounced gravity anomalies in Central Europe with peak-to-peak amplitude of about 70 mgal.

The scalar gravity anomalies along the flight trajectories have been derived from the airborne gravimeter taking into account platform recordings and data from the GPS-controlled Inertial Measurement Unit (IMU) Aerocontrol IIb. All common corrections have been performed on the raw gravity data. Due to problems in GPS recording, we used the IMU data only.

To verify the airborne gravity results, ground-based and satellite-derived gravity data have been used to compute local analytical gravity field models in a new methodological approach that allows the calculation of gravity anomalies at flight altitudes. For the most part there is a good agreement between the INS-airborne-derived and the independently modelled gravity anomalies, yielding best results of about 3.5 mgal RMS.

Keywords: airborne gravimeter, Inertial Measurement Unit (IMU), gravity anomalies, analytical gravity field model

1. Introduction

In 2006 the GFZ-owned LaCoste and Romberg airborne gravimeter S124 was upgraded by "Micro-g LaCoste" Company to the "Air Sea Dynamic Gravity Meter System II". It is now equipped with more sensitive platform accelerometers and single-axis fibre optic gyros, as well as new control and recording hard- and software including time synchronisation and additional platform control by GPS. The "Air Sea II" software is a fully automated system for controlling the gravimeter and its platform. It records all necessary raw data and calculates a filtered gravity signal corrected for cross coupling, Eötvös effect, and latitude changes.

For testing the performance of the upgraded gravimeter S124 and evaluating the newly updated software, an airborne gravity test campaign has been carried out in the northern part of Germany by GFZ Potsdam in autumn 2006 using the aircraft Cessna 404 of "Hansa Luftbild" Company, Münster, Germany.

We present the results of a profile, flown in both directions, SW to NE and NE to SW, at a nearly constant mean altitude of ~1100 m with a ground speed of ~230 km/h, crossing

pronounced gravity anomalies in Central Germany (Fig. 1) with a maximum peak-to-peak amplitude of about 70 mgal.

Fig. 1 Flight profile and related gravity anomaly points used for the validation procedure (3238 terrestrial points (brown dots); CHAMP-derived points at 200 km (small green squares) and 400 km altitude (large red squares); cf. further explanations in section 6.

Along the selected tracks the aircraft was navigated by autopilot supported by small corrections of the pilot. Only small turbulences occurred during the flight. The scalar gravity anomalies along the flight trajectories have been derived from the airborne gravimeter taking into account platform recordings and data from the GPS-controlled Inertial Measurement Unit (IMU) Aerocontrol IIb ("IGI" Company). All common corrections have been performed on the raw gravity data. Because of problems in GPS recording, we used IMU-processed data only.

For verification of the airborne gravity results, ground-based and satellite-derived gravity data have been used to compute local analytical gravity field models in a new methodological approach that allows the calculation of gravity anomalies at flight altitudes.

2. Hardware components

The airborne campaign has been carried out with the aircraft Cessna 404 of "Hansa Luftbild" Company, Münster, Germany. It was equipped with the upgraded LaCoste and Romberg "Air Sea Dynamic Gravity Meter System II" S124, the GPS-controlled IMU Aerocontrol IIb and two GPS receivers Novatel OEM-4 (Fig. 2).

77

78 **Fig. 2** LCR airborne gravimeter (left) and IMU composed of sensor and electronic unit (right)
79 mounted in Cessna 404.

80

81 **2.1 Airborne gravimeter**

82

83 The LaCoste and Romberg Air-Sea gravimeter is a highly damped spring-type gravimeter
84 based on the zero-length principle mounted in a gyro-stabilized platform with controlling and
85 data acquisition electronics (LaCoste, 1967; Valliant 1992). Its main technical parameters are:
86 Dimensions: 71x56x84 cm, Mass: 86 kg, Range: 12000 mgal, Drift: 3 mgal per month,
87 Accuracy: ~1 mgal, Recording rate: 1 Hz, Platform pitch: +/-22 deg, Platform roll: +/-25 deg

88

89 **2.2 GPS/IMU system Aerocontrol IIb**

90

91 The precise positioning of the sensor is performed by the GPS/IMU system AEROcontrol-IIb.
92 The AEROcontrol was developed especially for the precise determination of the position,
93 orientation and velocity of airborne sensors for photogrammetry and remote sensing, such as
94 airborne mapping cameras, airborne LiDAR systems or SAR. To obtain a sufficient accuracy
95 for a direct geo-referencing of these sensors, the AEROcontrol is designed to reach an
96 accuracy of 0.005° for the roll and pitch angle and 0.01° for the heading. The absolute
97 positioning accuracy depends on the actual GPS accuracy. The used dual frequency carrier
98 phase processing provides a positioning with an accuracy in the range of a few centimetres.
99 Although the quality of the final positioning solution depends on the momentary GPS
100 conditions, the coupling of GPS and inertial technology leads to an improvement of the
101 accuracy of the trajectory determination of an airborne sensor. The main improvements are:

- The IMU operates at a significantly higher data rate than GPS. For the described measurement campaign, the aircraft moving at a speed of 230 km/h (~125 kts), the distance between two GPS position measurements would be roughly 64 m for 1 Hz or 13 m for 5 Hz, respectively. For the data rate of the used IMU (50 Hz) the distance between two position measurements is 128 cm. To calculate the exact position in-between the measurements, a spline approximation is used.
- The orientation measurement of the IMU allows taking the position offset (lever arm effect) between the airborne gravimeter, the IMU and the phase center of the GPS antenna correctly into account.
- The trajectory including attitude and velocities is calculated from the IMU measurements with a so-called "strap down algorithm". The optimal combination of the GPS and the IMU information, including an estimation of the exact IMU calibration, is done in a Kalman filter process. The output of this process is a smoothed trajectory obtained from processing the data forward and backward in time.
- The IMU includes three accelerometers and two tuned gyroscopes with two sensitive axes each. Their properties are shown in Table 1. The signal processing takes place in a separate electronic unit that is mounted besides the IMU. The IMU-IIb provides a high-accuracy measurement of the angular rate and of the acceleration with an update rate of 50 Hz.

Table 1 Properties of the IMU-IIb

3. Airborne data treatment and processing

By neglecting horizontal acceleration the characteristics of the zero length spring-dynamic LaCoste and Romberg sea/air gravimeter can be described by the differential equation

$$g + \ddot{z} + b \cdot \ddot{B} + f \cdot \dot{B} + k \cdot B - c \cdot S = 0 \qquad (1)$$

with g = gravity; $\ddot{z}$ = vertical acceleration exerted on the gravimeter; B = displacement of the gravimeter test mass relative to the zero position of the meter case; S = spring tension; *b, f, k, c* = constants assuming linear gravimeter characteristics.

The first three terms g, $\ddot{z}$, and $b \cdot \ddot{B}$ of Eq. (1) result from gravitation and acceleration forces acting on the test mass. The term $f \cdot \dot{B}$ reflects the damping and $k \cdot B$ the restoring force of the spring tension. The term $c \cdot S$ represents the vertical force per unit mass at the centre of the test mass defined by the mechanical links when the mass is nulled (Meyer et al. 2003).

For the sea/air gravimeter the factor k equals zero since there is no restoring force. The damping factor f is rather large but constant. The beam will rapidly acquire its maximum velocity for a given unbalanced force acting on it. The term $b \cdot \ddot{B}$ becomes insignificant. The approximate linear equation for the LCR air/sea gravimeter is thus

$$g + \ddot{z} + f \cdot \dot{B} - c \cdot S = 0 \qquad (2)$$

with f = damping factor, traditionally called *K*-factor and c = calibration factor of the spring (Valliant 1992).

The spring tension is slowly adjusted by a feedback loop to prevent the beam from drifting too far away from equilibrium. Readings of the beam velocity $\dot{B}$ and spring tension can be done even when the beam is moving. The measurement becomes a combination of beam

velocity and spring tension and is up to first order independent of beam position (Olesen, 2003).

Considering the vertical accelerations, one has to take the cross coupling effect into account. Here the vertical acceleration causes the deflection of the lever arm and the horizontal acceleration acting after a certain phase shift causes an additional torque. Based on this fundamental theoretical background the equation for the LCR gravimeter can be derived.

3.1 Gravity variation derived from gravimeter and platform data (δgc)

According to Eq. (2) gravity from the gravimeter readings can be calculated by

$$\delta gc = (Bv \cdot Kf + ST \cdot STc + CC) \cdot Scf \tag{3}$$

with Kf = 0.10324 (K factor, a constant which is a function of the average beam sensitivity and the damping.), Bv = beam velocity, ST = spring tension, STc = 0.974 (spring tension coefficient), CC = cross coupling, Scf = 0.963 (scaling factor gravity).

3.2 Cross coupling gravity effect (CC)

Horizontal accelerations cause a deflection of the gravimeter's lever arm by an additional torque. Therefore, horizontal accelerations cause an additional vertical acceleration, the cross coupling effect, which must be corrected. The cross coupling effect depends on the magnitude and phase of the disturbing horizontal accelerations and the relationship between the reflection of the lever arm and vertical acceleration. This relationship is characterized by sensitivity and damping of the gravimeter (Torge, 1989).

The cross coupling effect has been calculated from the 5 so-called cross coupling monitors (Valliant, 1992). They are derived from beam position B and beam velocity Bv and the

horizontal platform accelerations measured by platform accelerometers in cross *Xacc* and long *Lacc* directions. The relations are: $VE = Bv^2$, $VCC = Lacc \cdot B$, $AX = Xacc \cdot Bv$, $AL = Lacc \cdot Bv$, $AX2 = Xacc^2 \cdot Bv$.

For each monitor the coefficients C_{VE}, C_{VCC}, C_{AX}, C_{AL} and, C_{AX2} were determined by "Micro-g LaCoste" Company using the cross correlation technique (LaCoste, 1973). With these coefficients the cross coupling effect can be determined as

$$CC = VE \cdot C_{VE} + VCC \cdot C_{VCC} + AX \cdot C_{AX} + AL \cdot C_{AL} + AX2 \cdot C_{AX2} \quad (4)$$

Fig. 3 shows the calculated and FIR filtered (cf. section 4.) cross coupling effect (*CC*)

Fig. 3 Calculated and FIR filtered cross coupling *CC*.

3.3 Calculation of the free air gravity anomaly (δgf)

For the determination of the free air gravity anomaly all disturbing accelerations must be subtracted from the cross coupling corrected gravity data δgc (cf. Eq. 3). The correction terms are: vertical aircraft acceleration (*Vacc*), the accelerations caused by platform tilt (δgT), Eötvös effect (δgE), latitude (δgL), and height (δgh), which leads to

$$\delta gf = \delta gc - Vacc - \delta gT - \delta gE - \delta gL - \delta gh \quad (5)$$

3.3.1 Vertical aircraft acceleration (*Vacc*)

The recorded IMU data were processed with the software "AEROoffice V. 5.1a". From this processing vertical speed, position (ϕ, λ, h) and heading angle α north are used for the evaluation of the airborne gravimeter data. By differentiation of the aircraft vertical speed the

vertical acceleration *Vacc* was calculated. Fig. 4 shows δgc, *Vacc,* and the difference signal $\delta gc1 = \delta gc - Vacc$ for a selected interval.

Fig. 4 Gravity δgc, vertical acceleration *Vacc* and difference signal $\delta gc1$.

3.3.2 Platforms tilt correction (δgT)

The gravimeter only measures the vertical component of gravity g_v if the gravity sensor axis is aligned to the vertical direction of the Earth's gravity field. If there is a misalignment between the two axes (angle θ), the measured gravity amounts to $g_m = g_v \cdot \cos\theta$ and the tilt signal $g_T = g_v(1-\cos\theta)$. The platform control minimizes the angle θ and hence the tilt signal. The tilt signal caused by remaining misalignments of the platform can be corrected according to Valliant (1992) by

$$\delta gT = \frac{Lacc^2 + Xacc^2 - (acce^2 + accn^2)}{2g} \qquad (6)$$

with accelerations: *Lacc* = long axis, *Xacc* = cross axis, *accn* = north direction, *acce* = east direction (Fig. 5).

Fig. 5 Calculated and FIR filtered platform tilt correction δgT.

3.3.3 Eötvös correction (δgE)

Because of the rotational platform motion relative to the Earth, a centrifugal acceleration and a Coriolis acceleration occur. The vertical component of these inertial accelerations, the

Eötvös effect, impacts the gravity measurements. It was determined according to Harlan (1968) as

$$\delta gE = v_{GS}{}^2 / a(1 - h/a - \varepsilon(1 - \cos^2\varphi(3 - 2\cdot\sin^2(\alpha))) + 2\cdot v_{GS}\cdot\omega_e\cdot\cos\varphi\cdot\sin\alpha \quad (7)$$

with v_{GS} = ground speed, a = semimajor axis ω_e = angular velocity, h = height above sea level, ϕ = latitude, α = angle heading north, and $\varepsilon = v_{GS}{}^2 / a\cdot\sin^2\varphi + 4\cdot v_{GS}\cdot\omega_e\cdot\cos\varphi\cdot\sin^2\varphi\cdot\sin\alpha$ (Fig. 6).

3.3.4 Height correction (δgh)

The height correction was calculated due to the free air gravity gradient for the height changes Δh (Fig. 6).

$$\delta gh = \Delta h\cdot 0.3086\cdot mgal/m \quad (8)$$

Fig. 6 Eötvös- δgE and height correction δgh.

3.3.5 Latitude correction δgL

For latitude correction the equation for normal gravity was used.

$$\delta gL = 9.78031846\cdot 10^5\cdot[5.278895\cdot 10^{-3}\cdot\sin(2\varphi) + 2.3462\cdot 10^{-5}\cdot\sin(4\varphi)] \quad (9)$$

4. Time synchronisation and filtering of the data series

For combining data sets of different instruments, the time shift was determined by cross correlation of the interpolated (10 Hz) time series (Olesen, 2002)

The corrected gravity data δgf are filtered with a FIR filter. This filter has 180 coefficients designed with a Blackman window (Fig. 7). Fig. 8 shows the filter response for a 1 sec sampling rate and a cut-off period of 180 sec (0.00556 Hz.)

Fig. 7 Filter coefficients FIR.

Fig. 8 Filter response FIR.

After applying this filter the data are smoothed by a moving average filter with a window length of 120 sec.

The spatial resolution of the gravity anomalies follows from the filter characteristics and the medium aircraft speed. For the applied filters and the medium aircraft speed of 64 m/s the spatial resolution is about 8 km at half wavelength.

Fig. 9 shows the FIR filtered and moving average smoothed gravity anomalies δgf_{FIR_Sm} of tracks 1a and 1b in comparison with the modelled gravity anomalies $\delta g_{M.}$ (cf. section 6)

Fig. 9 FIR filtered and moving average smoothed gravity anomalies δgf_{FIR_Sm} of track 1a and 1b in comparison with modelled gravity anomalies δg_M.

5. Positioning offset between airborne gravimeter and GPS antenna phase center

Depending on the length of the lever arm, the distance between the airborne gravity sensor (point A) and the phase center of the aircraft-mounted GPS antenna (point B), different velocities and accelerations acting in points A and B during the flight. Therefore, the GPS-

measured velocity and acceleration at point B (phase center of the GPS antenna) must be exactly transformed to point A (gravity sensor) for the exact determination of the vertical acceleration of the aircraft at the position of the airborne gravity sensor. If no IMU is used for the determination of the vertical acceleration of the aircraft (cf. section 2.2), the acceleration difference (lever arm error) must be calculated and corrected.

5.1 Positioning from GPS antennas to the airborne gravimeter

The flight-state of an aircraft can be monitored by using several GPS antennas fixed on the outside of the aircraft. The flight-state is usually represented by so-called "state angles" (heading, pitch, and roll). They are rotation angles between the body frame and the local horizontal coordinate frame of the aircraft. The axes of the body frame are selected as follows: the x^b axis points out the nose, the y^b axis points to the right parallel to the wing, and the z^b axis points out the belly to form a right-handed coordinate system, where b denotes the body frame. The body frame can be rotated to be aligned to the local horizontal frame in a positive, right-handed sense, which is outlined in three steps. First, the body frame is rotated about the local vertical downward axis z^b by angle ψ (heading). Then the body frame is rotated about the new y^b axis by angle θ (pitch). Finally, the body frame is rotated about the new x^b axis by angle ϕ (roll). In the local horizontal coordinate system, the heading is the azimuth of axis x^b of the body frame, the pitch is the elevation of axis x^b of the aircraft and the roll is the elevation of axis y^b of the aircraft (Fig. 10). Note that the directions of the axis x^b and the velocity vector of the aircraft are usually not the same. Through kinematic positioning, the three flight state monitoring angles ψ, θ and ϕ can be computed (Cohen, 1996 and Xu, 2007). However, the derivations hold for simplified assumptions and the formulae are not generally valid. GPS is used to determine the position and velocity of the

antennas; however, what one needs is the position and velocity (as well as acceleration) of the airborne gravimeter. This paper will provide a general algorithm of flight-state monitoring and derive the position and velocity (as well as acceleration) of the airborne gravimeter. This is significant for kinematic platform monitoring practice including airborne-gravimetry.

Fig. 10 Coordinate systems.

In the following, the derivation of the algorithm is described in detail.

The geometric center point of the three antennas is defined by

$$X^b(c) = \frac{1}{3}(X^b(1) + X^b(2) + X^b(3)) \tag{10}$$

while the origin of the body frame to the center point is translated by

$$X^b(1) - X^b(c),\ X^b(2) - X^b(c),\ X^b(3) - X^b(c)\,. \tag{11}$$

where $X^b(1), X^b(2), X^b(3)$ are three coordinate vectors of the antennas in the body frame. According to the definition of the body frame and horizontal coordinate system, one has (cf. Xu, 2007)

$$X^h(i) = R_1(\phi)R_2(\theta)R_3(\psi)X^{db}(i), \quad i = 1,2,3 \tag{12}$$

where $X^h(i)$ are coordinate vectors in local horizontal frame and denote $X^{db}(i)=X^b(i)-X^b(c)$. The rotation is defined by

$$\begin{aligned} R &= R_1(\phi)R_2(\theta)R_3(\psi) \\ &= \begin{pmatrix} R_{11} & R_{12} & R_{13} \\ R_{21} & R_{22} & R_{23} \\ R_{31} & R_{32} & R_{33} \end{pmatrix} \\ &= \begin{pmatrix} \cos\theta\cos\psi & \cos\theta\sin\psi & -\sin\theta \\ \sin\phi\sin\theta\cos\psi - \cos\phi\sin\psi & \sin\phi\sin\theta\sin\psi + \cos\phi\cos\psi & \sin\phi\cos\theta \\ \cos\phi\sin\theta\sin\psi - \sin\phi\cos\psi & \cos\phi\sin\theta\sin\psi - \sin\phi\cos\psi & \cos\phi\cos\theta \end{pmatrix} \end{aligned} \tag{13}$$

313 The coordinate vectors of the three GPS antennas and the gravimeter
314 ($X^b(1), X^b(2), X^b(3), X^b(4)$) are well known due to the body coordinate system definition and
315 measurements after mounting of the instruments. The coordinates of the three antennas in the
316 global coordinate system (e.g. ITRF2000) are known through GPS adjustment and are
317 denoted by ($X^g(1), X^g(2), X^g(3)$). All coordinate vectors have three components *x*, *y*, *z*. The
318 geometric center of the three antennas in global GPS frame is

319 $$X^g(c) = \frac{1}{3}(X^g(1) + X^g(2) + X^g(3)) \tag{14}$$

320 Using the geometric center point as origin, a local horizontal frame can be defined and the
321 three known GPS positions $X^g(1), X^g(2), X^g(3)$ can be transformed into the local horizontal
322 frame by

323 $$X^h(i) = R_0 X^g(i), \quad i = 1,2,3 \tag{15}$$

324 $$R_0 = \begin{pmatrix} -\sin\varphi\cos\lambda & -\sin\varphi\sin\lambda & \cos\varphi \\ -\sin\lambda & \cos\lambda & 0 \\ \cos\varphi\cos\lambda & \cos\varphi\sin\lambda & \sin\varphi \end{pmatrix}. \tag{16}$$

325 where φ and λ are the geodetic latitude and longitude of the geometric center point of the three
326 antennas in the global GPS frame (cf. Xu 2007).
327 Then the flight state monitoring angles can be determined by Eq. 12. Altogether, there are 9
328 equations and three angular variables. Because of the three angular unknowns and arguments
329 of sinus and cosines functions which are multiplied to each other, the problem can not be
330 solved in a straightforward way. However, there exists a unique set of solutions which has
331 been found in different ways by different authors many years ago (cf. Sanso, 1973 and 1976).
332 After the flight-state angles have been determined, the coordinates of the points of interest,
333 e.g., the gravimeter, can be computed by

$$X^h(4) = R_1(\phi)R_2(\theta)R_3(\psi)(X^b(4) - X^b(c)) \quad (17)$$

where $X^b(4)$ is the coordinate vector of the point of interest in body frame and $X^h(4)$ is the coordinate vector of the point of interest in the local horizontal frame. $X^h(4)$ can be transformed into the global GPS frame. In this way, the coordinate vector of the point of interest in the global GPS frame can be obtained. Furthermore, the velocity of the point of interest can be obtained by numerical differentiation.

5.2 Velocity of the airborne gravimeter deduced from velocities of GPS antenna

Velocities of the three GPS antennas can be determined by using Doppler observations. The problem of the velocity determination of the airborne gravimeter can be outlined as follows. In a fixed body with known positions and velocities of three points the search for the velocity of a known point in the body must be carried out. The problem turns out to be a geometric one. One has three independent distance relations of

$$\begin{aligned}
(x_4 - x_1)^2 + (y_4 - y_1)^2 + (z_4 - z_1)^2 &= d_{41}^2 \\
(x_4 - x_2)^2 + (y_4 - y_2)^2 + (z_4 - z_2)^2 &= d_{42}^2 \\
(x_4 - x_3)^2 + (y_4 - y_3)^2 + (z_4 - z_3)^2 &= d_{43}^2
\end{aligned} \quad (18)$$

where the indices 1, 2, 3, 4 are used to identify the number of the points. The distance between points i and j is represented by d_{ij}. Differentiating Eq. 18 with respect to time t, one obtains

$$\begin{aligned}
(x_4 - x_1)(\dot{x}_4 - \dot{x}_1) + (y_4 - y_1)(\dot{y}_4 - \dot{y}_1) + (z_4 - z_1)(\dot{z}_4 - \dot{z}_1) &= 0 \\
(x_4 - x_2)(\dot{x}_4 - \dot{x}_2) + (y_4 - y_2)(\dot{y}_4 - \dot{y}_2) + (z_4 - z_2)(\dot{z}_4 - \dot{z}_2) &= 0 \\
(x_4 - x_3)(\dot{x}_4 - \dot{x}_3) + (y_4 - y_3)(\dot{y}_4 - \dot{y}_3) + (z_4 - z_3)(\dot{z}_4 - \dot{z}_3) &= 0
\end{aligned} \quad (19)$$

These are three linear equations with three unknowns $\dot{x}_n$, $\dot{y}_n$, $\dot{z}_n$ of velocity components and there exists a unique set of solutions. In this way the velocity of the gravimeter can be determined. Acceleration of the airborne gravimeter can be obtained by numerical differentiation of the velocity series.

5.3 Numerical example of the lever arm effect

To demonstrate the influence of the lever arm effect on the accelerations, a numerical example based on real data is presented below. The calculations has been done according to the outlined theory using Eq. 19 for a flight track with 1 GPS antenna and a distance (lever arm) between GPS antenna and gravity sensor expressed by x4= -2.209 m, y4= 0.325 m, z4=-1.082 m. To compute the velocity and acceleration at the gravimeter position only changes of the pitch angle θ (lever arm 2.209 m) were taken into account. Changes in roll angle ϕ (roll causes small accelerations because of the small lever arm of y= 0.325m) and heading angle ψ (heading causes the same vertical accelerations for GPS and gravimeter) were set to zero and neglected.

The following steps were carried out:

- transformation of the GPS antenna position in the global GPS frame $X^g(1)$ to the local horizontal frame $X^h(1)$ by using Eq. 15 and 16,
- determination of the flight state monitoring angles ψ, θ and ϕ (local horizontal frame) using Eq. 12 and 13,
- calculation of the coordinate vector of gravimeter (local horizontal frame) using Eq. 17,
- determination of velocity of the gravimeter using Eq. 18 and 19, and
- determination of the acceleration of the gravimeter by numerical differentiation.

The height profile h of this example track is shown in Fig. 11a). The calculated height differences δh between antenna and airborne gravimeter and the associated vertical acceleration differences (lever arm effect) δg_La are given in Figs. 11b) and 11c).

These height differences will not significantly affect the results since they are within the height precision requirement (<1m). However, the lever arm effect δg_La is quite noticeable and could amount up to 1000 mgal. It can be considerably reduced by filtering with the FIR filter described in section 4. The filtered lever arm effect δg_LaF is shown in Fig. 11c. It reaches at intervals t1 and t3 up to +/-20 mgal. Such large height changes δh (pitch angle θ) are infrequent during a flight campaign but they clearly demonstrate that a large lever arm effect cannot be neglected. The height changes (pitch angle θ) at interval t2 are realistic and can cause a lever arm effect of some mgal. The larger the lever arm, the larger is δg_La. If the cut-off frequency of the applied filter is reduced (in our example 180 sec) to, e.g., 120 sec, which correspond to a higher resolution in space, δg_LaF becomes larger. In conclusion, it can be said that the correction of the lever arm effect caused by the different location of the GPS antenna and the airborne gravimeter within the aircraft should be a standard algorithm in the evaluation of airborne gravity data.

Fig.11 a) height profile h, b) height differences δh and c) acceleration differences (lever arm effect) δg_La and δg_LaF of the example flight track

6. Validation of the airborne results

For an independent check of the airborne gravity results, a new approach has been applied. It is based on the computation of 3D regional analytical gravity field models in line with a so-called space value problem approach (SVP) (Schäfer, 2003). This means the original point data from the positions where they were observed are directly taken into account. In this study, ground and satellite data are used.

On the basis of these independent data sources regional analytical models have been computed. Afterwards the gravity anomaly predictions obtained from these independent models are compared with the airborne observations at the same 3D points.

6.1 Analytic model

The computed regional analytical models have been derived in the context of the so-called linear integral representation approach (Strakhov et al., 2003) and are called SLINTAX (Single-layer Linear INTegral ApproXimation) models. The basic concept can be briefly summarized as follows.

Since the gravity disturbing potential $T(x)$ at a certain point in space is harmonic outside a sphere containing the attracting masses, i.e., at $r>R_0$, it can be represented in spherical coordinates by the following integral representation:

$$T(x)=\frac{R_0^2}{4\pi}\int_0^{2\pi}\int_0^{\pi}\frac{\sigma(\tilde{\vartheta},\tilde{\varphi})\sin\tilde{\vartheta}\,d\tilde{\varphi}\,d\tilde{\vartheta}}{R(\xi-x)}+\frac{R_0^2}{4\pi}\int_0^{2\pi}\int_0^{\pi}\frac{w(\tilde{\vartheta},\tilde{\varphi})(R_0-r\cos\vartheta')\sin\tilde{\vartheta}\,d\tilde{\vartheta}\,d\tilde{\varphi}}{R^3(\xi-x)}, \qquad (20)$$

with

$$R(\xi-x)=(R_0{}^2-2R_0r\cos\vartheta'+r^2)^{1/2}, \qquad \xi=(R_0\cos\tilde{\varphi}\sin\tilde{\vartheta},R_0\sin\tilde{\varphi}\sin\tilde{\vartheta},R_0\cos\tilde{\vartheta}),$$
$$x=(r\cos\varphi\sin\vartheta,r\sin\varphi\sin\vartheta,r\cos\vartheta), \qquad \cos\vartheta'=\sin\vartheta\sin\tilde{\vartheta}\cos(\varphi-\tilde{\varphi})+\cos\vartheta\cos\tilde{\vartheta}.$$

The function $\sigma(\vartheta,\varphi)$ represents the density of a single layer distributed over the sphere of radius R_0, the function $w(\vartheta,\varphi)$ is the density of a double layer (distributed over the same sphere) and $R(\xi - x)$ is the distance between the current point ξ and the observation point x. Differentiating the right-hand side of the above equation $T(x_i)$ with respect to various coordinates, the integral representations of the respective derivatives of $T(x)$ can be obtained, e.g., $\delta g_r = \frac{\partial T}{\partial r}$.

$$T(x) = \frac{1}{4\pi}\int_0^{2\pi}\int_0^{\pi}\left(\frac{1}{R(\xi - x)}\cdot\frac{\partial T(\xi)}{\partial r} - T(\xi)\frac{\partial}{\partial r}\left(\frac{1}{R(\xi - x)}\right)\right)\sin\vartheta d\vartheta d\varphi. \qquad (21)$$

We consider in this study integral representations with single layer density distributions, i.e., one has to determine the unknown single layer density distribution $\sigma(\vartheta,\varphi)$. The parameterized single layer density will be determined as the solution of a system of linear algebraic equations with a full design matrix. For more details see Strakhov et al. (2003).

6.2 Validation data

The location of flight track 1 was selected in order to fly over distinguished and well-known gravity anomalies in an area with good terrestrial gravity data coverage complemented by available satellite data (blue line in SW-NE direction in Fig. 1).

For the computation of 3D regional analytical gravity field models point data from three different data sources were incorporated:

A) terrestrial (ground) gravity data points (BKG data base, 2007)

The terrestrial data were selected from the BKG data base by choosing all gravity point data within a lateral stripe of about 18.5 km width (4' to each side; see: light blue stripe in Fig. 1) along the track with a length of about 320 km (with edge points at 51.25 N, 10.25 E and 53.75 N, 12.62 E). This yields 3238 gravity points belonging to the area of approx. 6000 km^2 inside the stripe that is just below the track (about one gravity point per 1.8 km^2).

B) GPS-levelling data (BKG data base, 2007)

We incorporated the data from 895 GPS/levelling points from the BKG data base, providing 895 approximate values of the disturbing gravity potential T at the Earth's surface by means of Brun´s formula (Heiskanen & Moritz, 1967) (red triangles in Fig. 12).

C) CHAMP gravity disturbing potential (Gerlach, 2005)

For our study, the Technical University Munich provided gravity disturbing potential values for the European territory obtained from processing two years of kinematic orbits of the CHAMP satellite mission with the energy balance approach (Gerlach et al., 2003) using the kinematic orbits given by Svehla & Rothacher (2004). We selected only those points from all available data over Europe which are closest to the arithmetic average within spatial "voxels" of 1° x 1.5° and 10 km thickness between 380 km and 430 km altitude in the area between 44 N–59 N and 0–21 E. This yields a subset of 896 irregularly distributed CHAMP gravity disturbing potential values (black dots in Fig 12).

6.3 Computing method and results

We applied the following step-by-step procedure:

1. Derivation of Slintax-*T* disturbing potential model using a total of 1791 *T* values being the sum of 895 point data from (B) and 896 point data from (C). The resulting model of this step is illustrated in Figs. 12 a) and b). This long-wavelength 3D disturbing potential model is valid over Germany for the ellipsoidal height interval from CHAMP altitude about 430 km down to the Earth's surface.
2. Computation of the radial derivatives δg_r from the 3D-Slintax-T model, obtained at the previous step in a number of points that have been selected in the following way:
   a) at 200 km altitude in a grid with 0.3° x 0.45°; and selecting those 46 points belonging to the area within a lateral stripe of ~ 111 km (30' to each side) along the 320 km-track 1 (green squares in Fig. 1)
   b) at 400 km altitude in a grid with 0.5° x 0.75°; and selecting those 42 points belonging to the area within a lateral stripe of ~ 222 km (60' to each side) along the 320 km-track 1 (red open squares in Fig. 1), yielding altogether 88 gravity anomalies δg_r
3 Computation of a Slintax-δg_r model based on 3326 gravity anomalies resulting:
   a) from the second step (88 points with gravity disturbance δg_r values), and,
   b) from 3238 original terrestrial gravity values g from (A), yielding 3238 δg_r values (brown dots in Fig. 1) (The radial component of the latter was estimated assuming that the direction of the g vector coincides roughly with that of the normal gravity vector $\boldsymbol{\gamma}$.)

The final approximation accuracies (observed minus modelled) for both Slintax models derived applying the space-value problem (SVP) approach are given in Table 2.

Table 2 Accuracy observed minus modelled gravity anomalies

Once the coefficients describing the single-layer density distribution of the Slintax models are determined one can easily compute gravity functionals at any location within the range of the model's validity, e.g., gravity anomalies at the aircraft flight elevations or in nadir points on the ground or at satellite altitudes. The calculated gravity anomalies at track 1 (δg_M) are shown in Fig. 9.

The standard deviation between the IMU-airborne-derived (δgf_{FIR_SM}) (Fig. 9) and the Slintax-modelled gravity disturbances (δg_M) based on 10501 evaluation points is about 5 mgal along track 1a and about 3.5 mgal along track 1b (flown in the opposite direction at the same mean altitude of about 1100 m) The standard deviation of the difference between the gravity anomalies (δgf_{FIR_SM}) of track 1a and 1b (Fig. 9) yields 5.3 mgal. Hence, the deviation of the airborne gravity anomalies from the Slintax-modelled ones is of the same order as the intercomparison of the anomalies obtained from the forward (1a) and backward (1b) flights.

Based on the derived analytical Slintax-*T* model, synthesized disturbing potential field values have been calculated at different altitudes. Examples of such synthesis are documented in Fig. 12.

One can clearly see the real 3D nature of the Slintax models and the field diminution as a function of altitude: the higher the elevation the smoother are the anomaly patterns.

a) **b)**

Fig 12 Disturbing potential Slintax-T model at different altitudes a) h=0 m and b) h=10 km. The synthesis has been performed at 111474 grid points 1' x 1.5' at each elevation level.

7. Conclusions

- The upgraded S124 is easy to handle and fulfils the requirements of a state-of-the-art airborne gravimeter.
- There is a good agreement between the IMU-airborne-derived and the independently modelled gravity anomalies.
- This confirms that the evaluation of airborne data based on a GPS-controlled IMU data treatment provides very reasonable results for airborne gravity surveys along tracks of some hundred kilometres length.
- Since nowadays the positioning data is commonly derived by taking into account the GPS data only, a significant improvement of airborne gravity results is expected from a combination of GPS and IMU.
- The correction of the lever arm effect should be a standard procedure in the evaluation of airborne gravity data.
- A space value problem approach (SVP) for validating und verifying airborne data has been presented. It allows to check the airborne gravimeter performance by means of independent terrestrial and satellite gravity data without modifying the original data by gridding procedures such as up- or downward continuation to certain reference surfaces, as it is usually done when solving boundary value problems (BVP). This approach can be recommended for testing airborne gravimeters “on the fly” in areas that are distinguished by a good terrestrial gravity data coverage and where satellite gravitational functionals are available.

References

551 Cohen CE (1996) Altitude determination. Parkinson BW, Spilker JJ (eds) Global Positioning
552 System: Theory and applications, Vol. II
553 Gerlach C, Földvary L, Svehla D, Gruber T, Wermuth M, Sneeuw N, Frommknecht B,
554 Oberndorfer H, Peters T., Rothacher M, Rummel R, Steigenberger P (2003) A CHAMP-
555 only gravity field model from kinematic orbit using the energy integral, Geophysical
556 Research Letters, AGU, 30(20), 2037, DOI:10.1029/2003GL018025
557 Gerlach C (2005) Personal communication (E-Mail), August 26, 2005
558 Harlan RB (1968) Eötvös correction for airborne gravimetry, J. Geophys. Res. 3, 4675-4679
559 Heiskanen WA, Moritz H (1967) Physical Geodesy, W.H.Freeman, San Fransisco
560 LaCoste LBJ (1967) Measurement of Gravity at Sea and in the Air. Rev. of Geophys. 5, 477-
561 526
562 Meyer U, Boedecker G, Pflug H (2003) ANGEL Airborne Navigation and Gravimetry
563 Ensemble & Laboratory Introduction and First Airborne Tests, Scientific Technical Report
564 GFZ Potsdam, ISSN 1610-0956
565 Olesen A (2003) Improved airborne scalar gravimetry for regional gravity field mapping and
566 geoid determination, Technical Report No. 24, National Survey and Cadastre – Denmark
567 (KMS), ISSN 0908-2867
568 Sanso F (1973) An Exact Solution of the Roto-translation Problem, Photogrammetria,
569 Elsevier Publishing Company, Amsterdam, N. 29, 203-216
570 Sanso F (1976) A further account of roto-translations and the use of the method of
571 conditioned observations, Rendiconti dell Accademia Nazionale dei Lincei (Classe di
572 Scienze fisiche, metematiche e naturali), Serie VIII, Vol. 60, N. 2, Roma
573 Schäfer U (2003) Towards the Unification of European Height Systems using Analytical
574 Models of the Earth's Gravity Field, in: „Analytical Representation of Potential Field Ano-

malies for Europe (AROPA)“, Workshop Proceedings, ECGS Cahiers, vol. 20, Luxembourg, 131-141

Strakhov VN, Kerimov IA, Stepanova IE, Strakhov AV (2003) The Linear Integral Representation Method as the Main Method for Constructing Linear Analytical Approximations of Gravity Field Elements: Main Modifications and Practical Use, in: „Analytical Representation of Potential Field Anomalies for Europe (AROPA)“, Workshop Proceedings, ECGS Cahiers, vol. 20, Luxembourg, 87-93

Svehla D, Rothacher M (2003) Kinematic Precise Orbit Determination for Gravity Field Determination, in: Sansò F (ed.) A Window on the Future of Geodesy, International Association of Geodesy Symposia, vol. 128, Springer Berlin Heidelberg, 181-188

Torge W (1989) Gravimetry, Walter de Gruyter, Berlin New York

Valliant H (1992) The Lacoste & Romberg air/sea gravimeter: an overview. In CRC Handbook of Geophysical Exploration at Sea, Boca Raton Press

Xu G (2007) GPS - Theory, Algorithms and Applications, 2nd Edition, Springer Verlag

Fig. 5

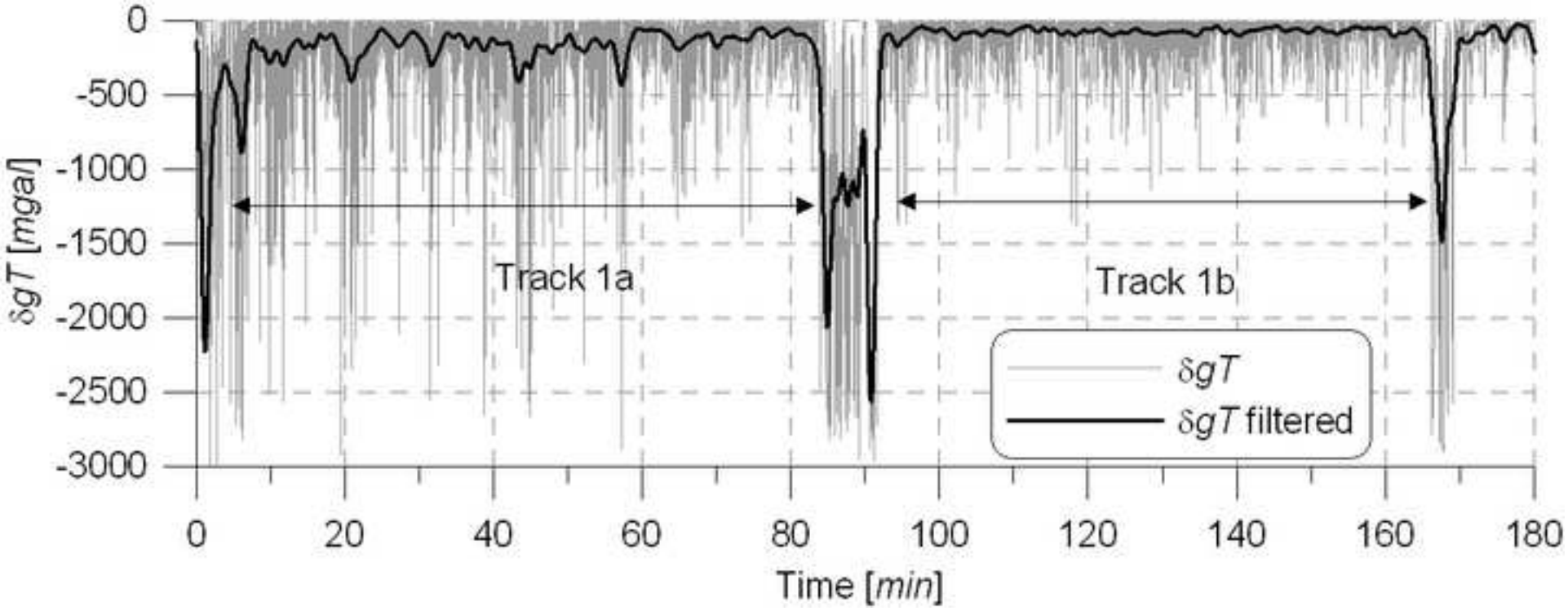
0
-500
-1000
-1500
-2000
-2500
-3000
δgT [mgal]
Track 1a
Track 1b
δgT
δgT filtered
0
20
40
60
80
100
120
140
160
180
Time [min]

Fig. 6

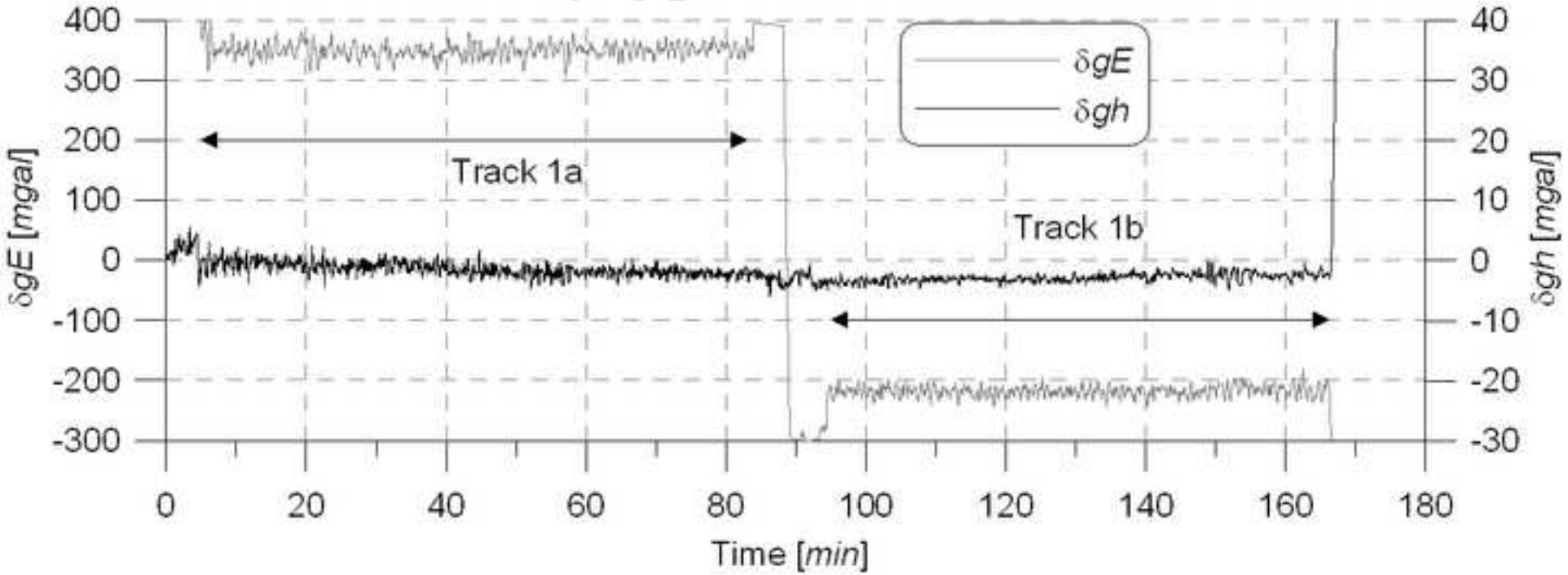
δgE
δgh
Track 1a
Track 1b
δgE [mgal]
δgh [mgal]
Time [min]
400
300
200
100
0
-100
-200
-300
40
30
20
10
0
-10
-20
-30
0
20
40
60
80
100
120
140
160
180

Fig. 7

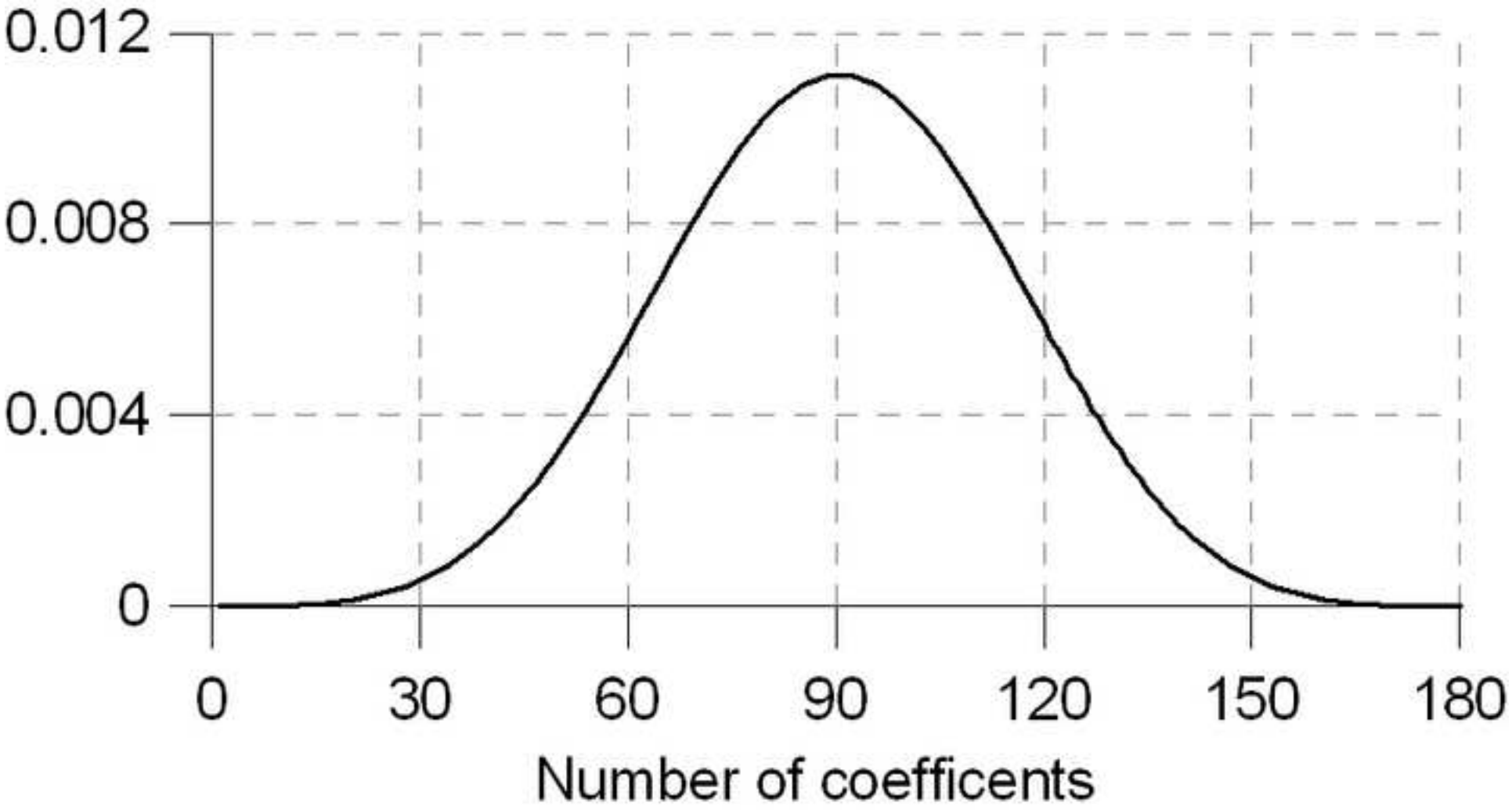

Fig. 8

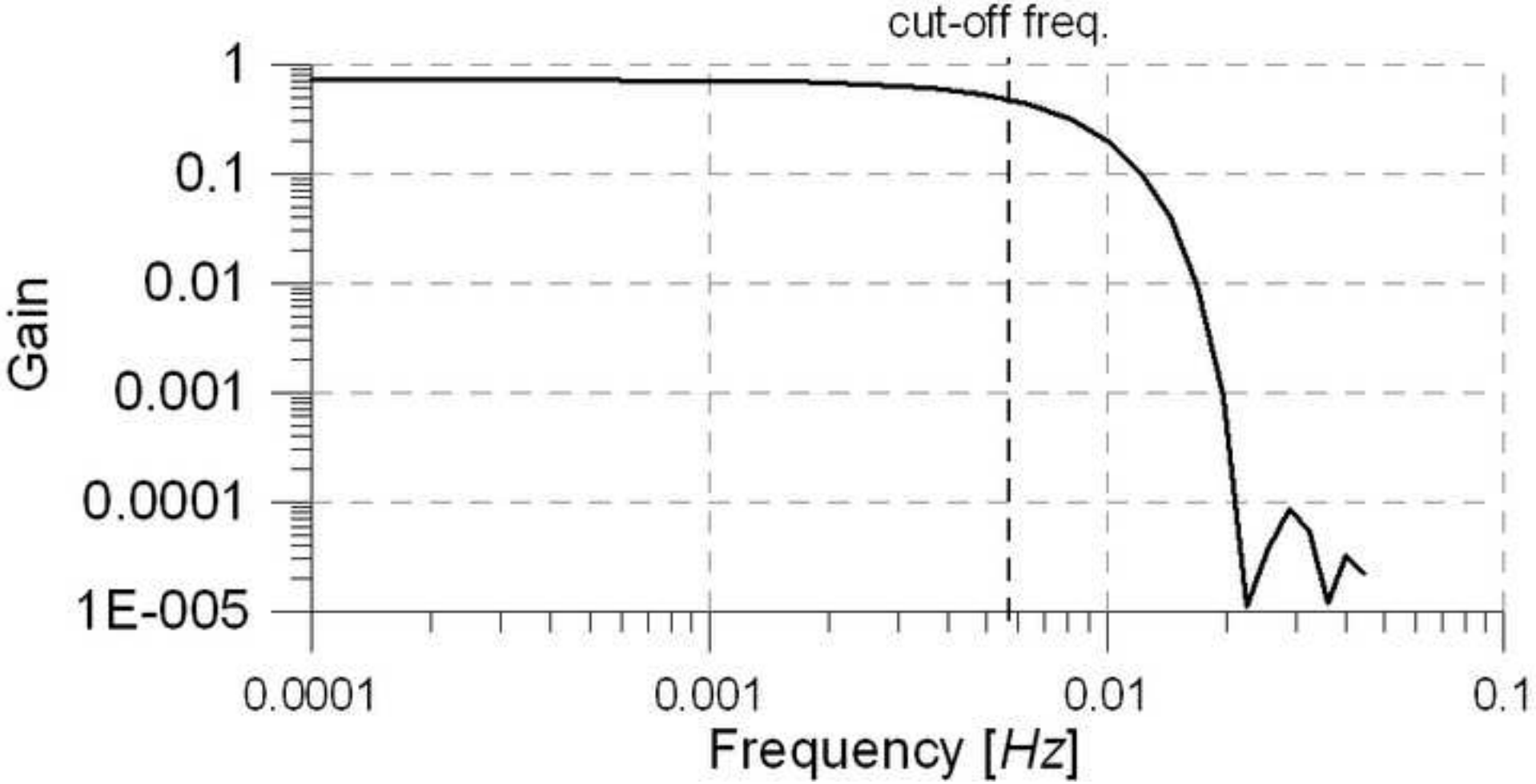
cut-off freq.
1
0.1
0.01
0.001
0.0001
1E-005
Gain
0.0001
0.001
0.01
0.1
Frequency [Hz]

Fig. 9

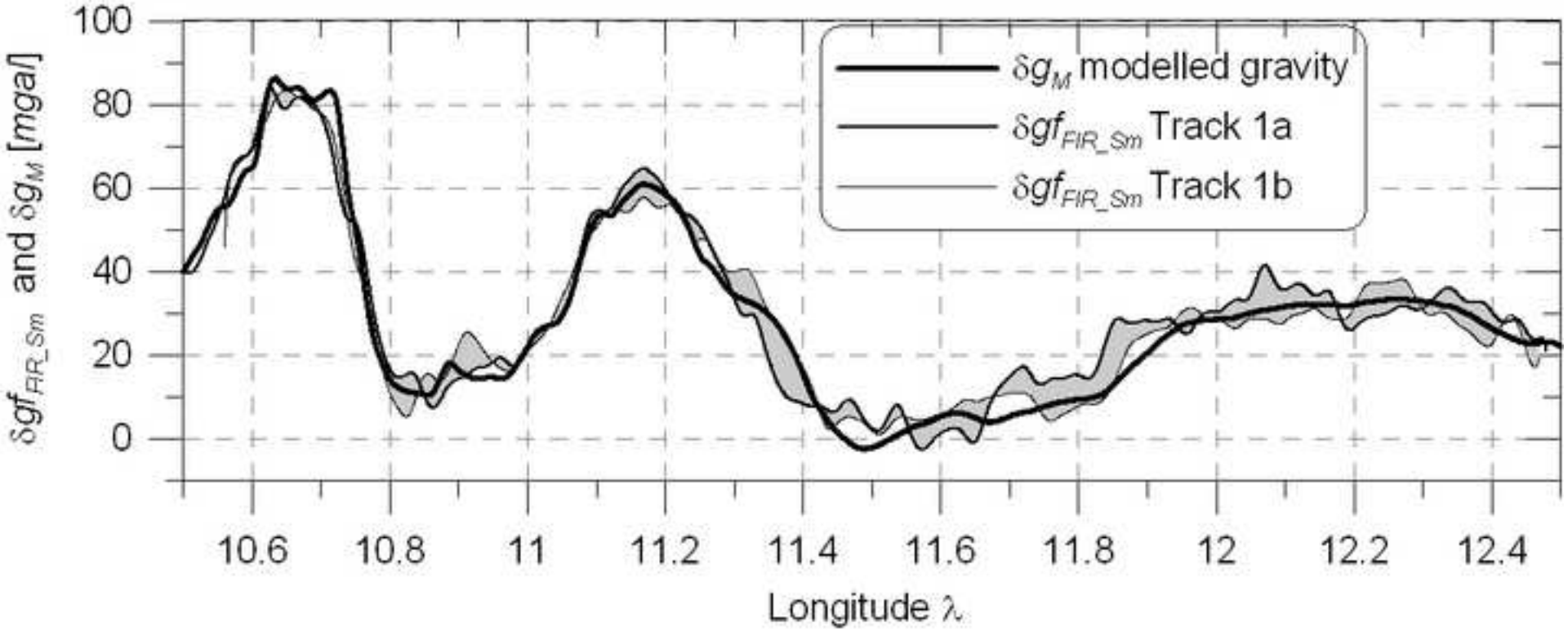
100
80
60
40
20
0
δgf_{FIR_Sm} and δg_M [mgal]
10.6
10.8
11
11.2
11.4
11.6
11.8
12
12.2
12.4
Longitude λ
δg_M modelled gravity
δgf_{FIR_Sm} Track 1a
δgf_{FIR_Sm} Track 1b

Fig. 10

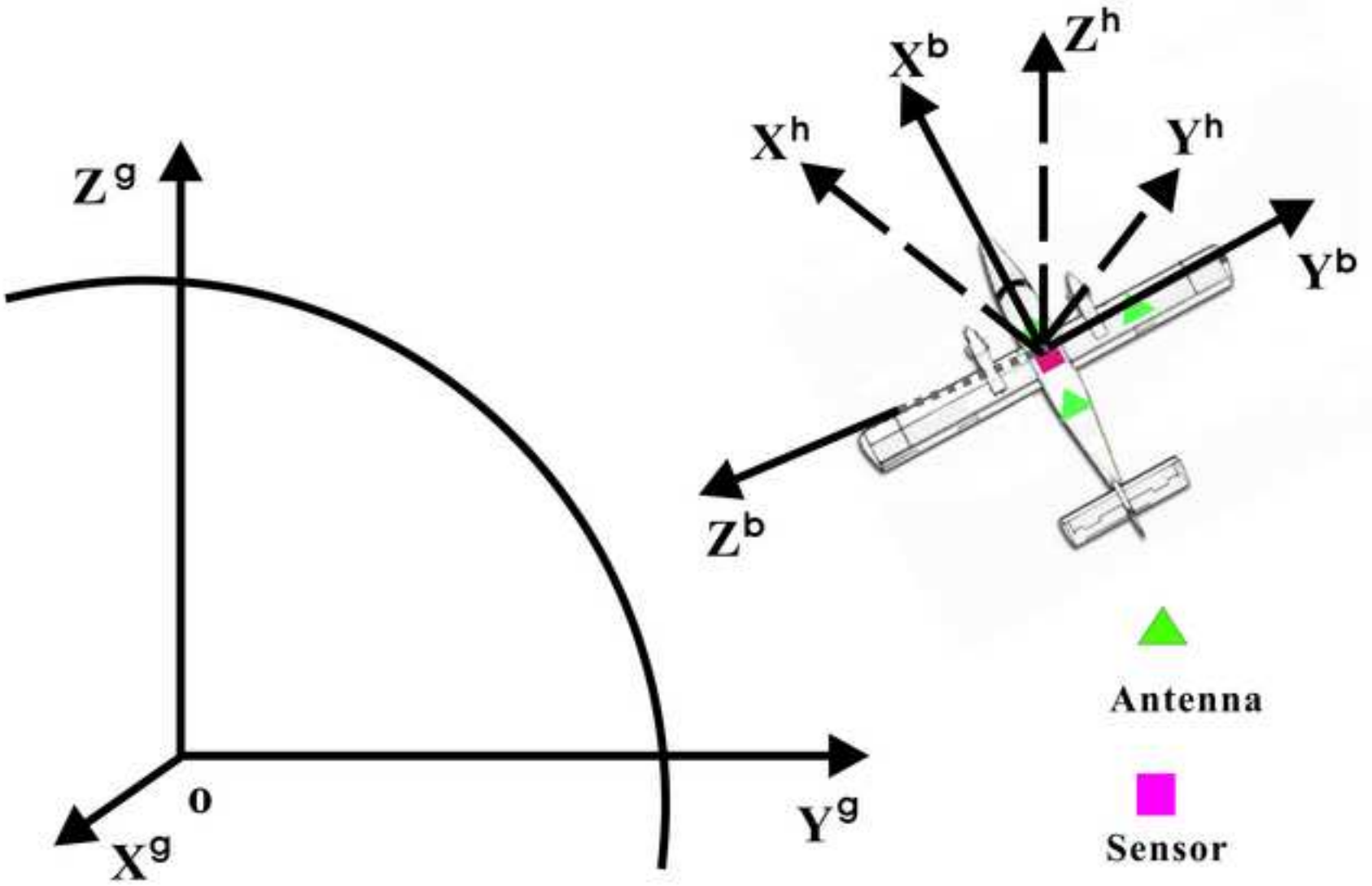

Fig. 11

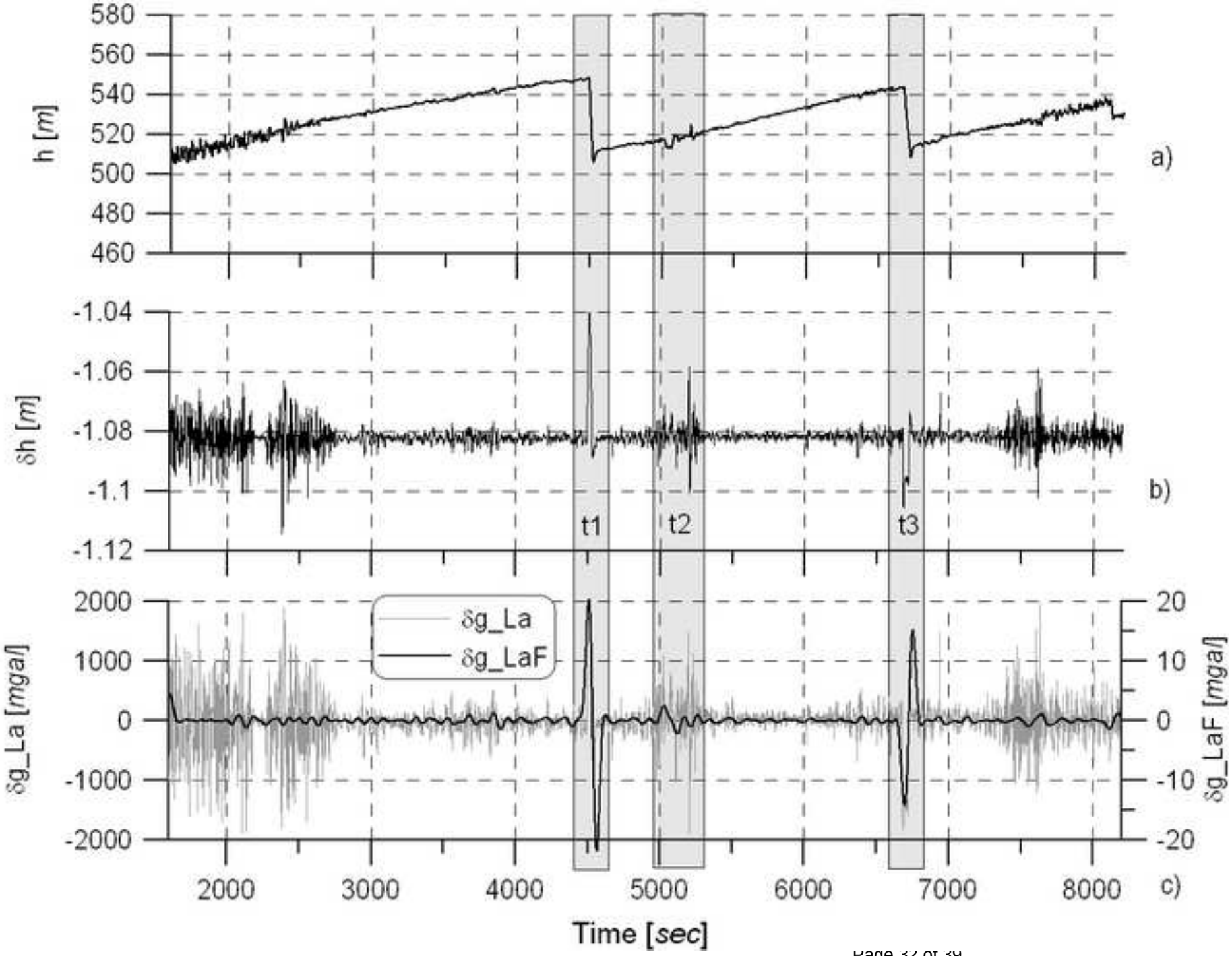
h [m]
580
560
540
520
500
480
460
a)
δh [m]
-1.04
-1.06
-1.08
-1.1
-1.12
t1
t2
t3
b)
δg_La
δg_LaF
δg_La [mgal]
δg_LaF [mgal]
2000
1000
0
-1000
-2000
20
10
0
-10
-20
2000
3000
4000
5000
6000
7000
8000
c)
Time [sec]

Fig. 12a-b

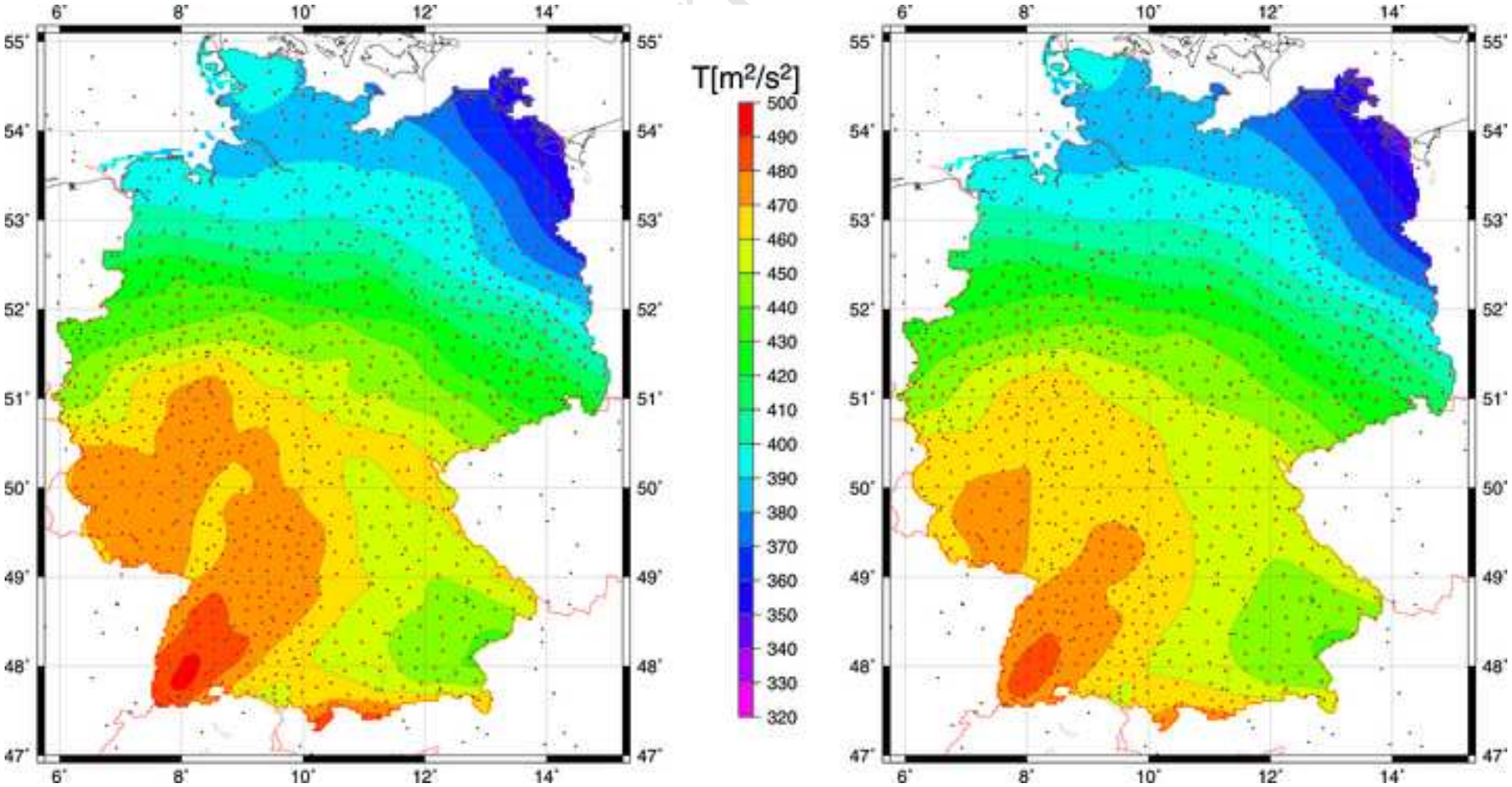
6°
8°
10°
12°
14°
55°
54°
53°
52°
51°
50°
49°
48°
47°
T[m²/s²]
500
490
480
470
460
450
440
430
420
410
400
390
380
370
360
350
340
330
320

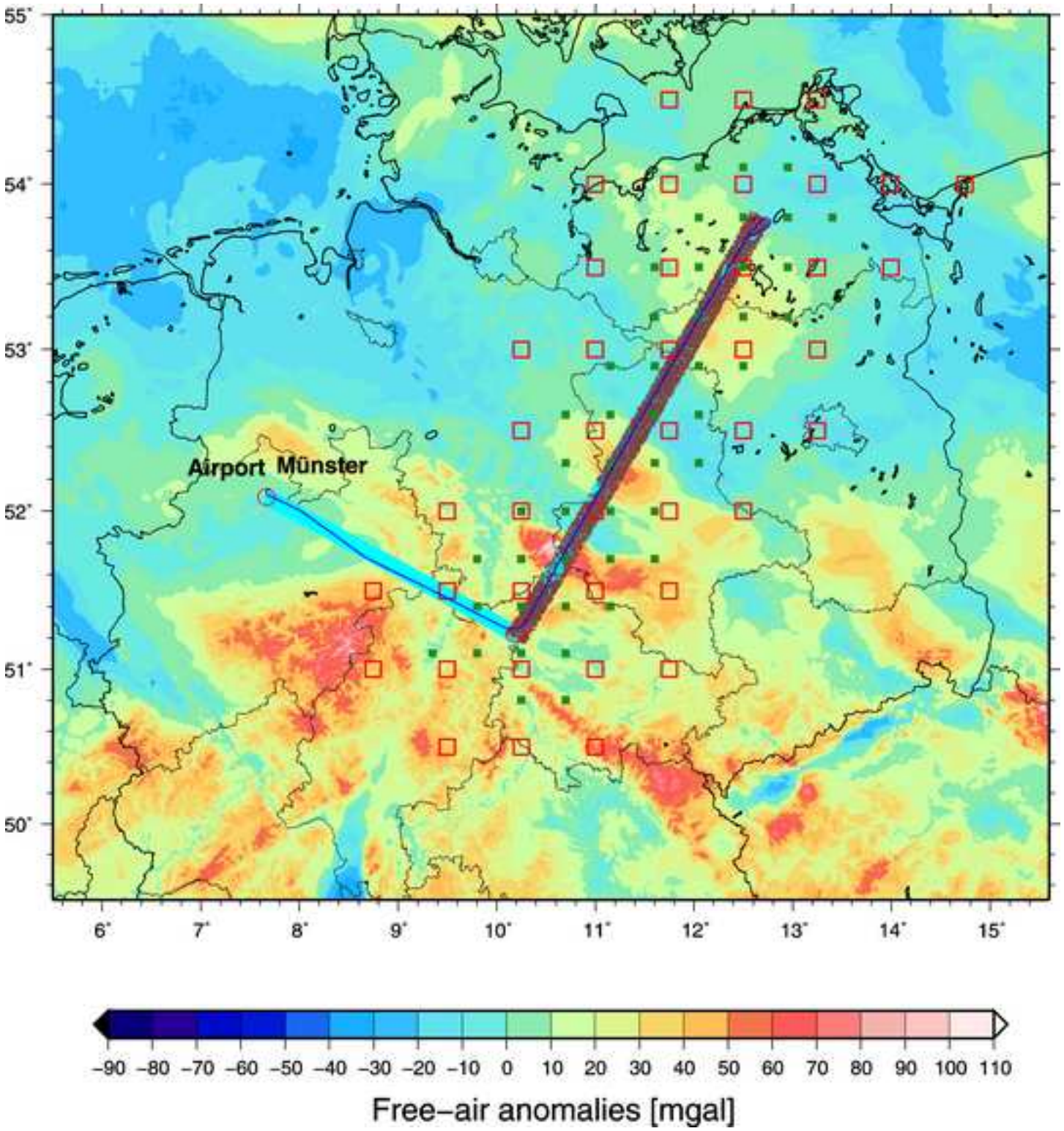

Fig. 3

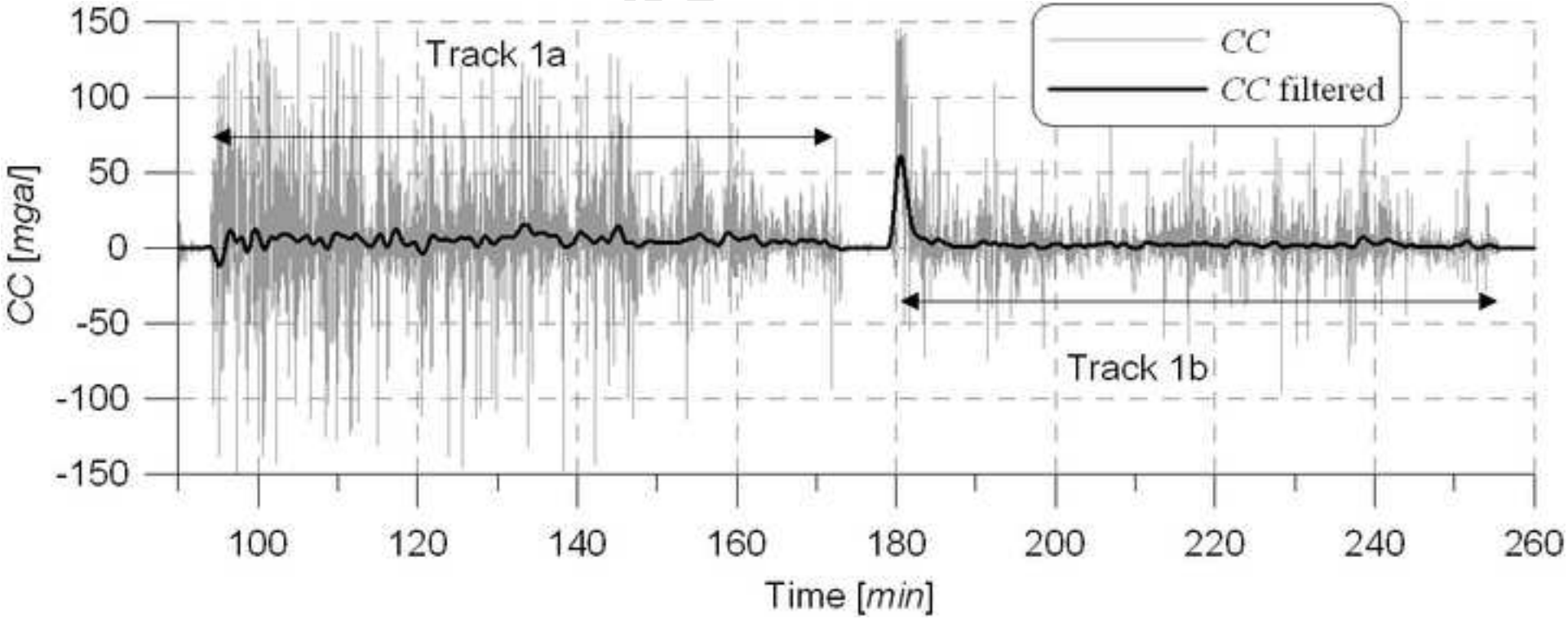
Track 1a
Track 1b
CC
CC filtered
CC [mgal]
Time [min]
150
100
50
0
-50
-100
-150
100
120
140
160
180
200
220
240
260

Fig. 4

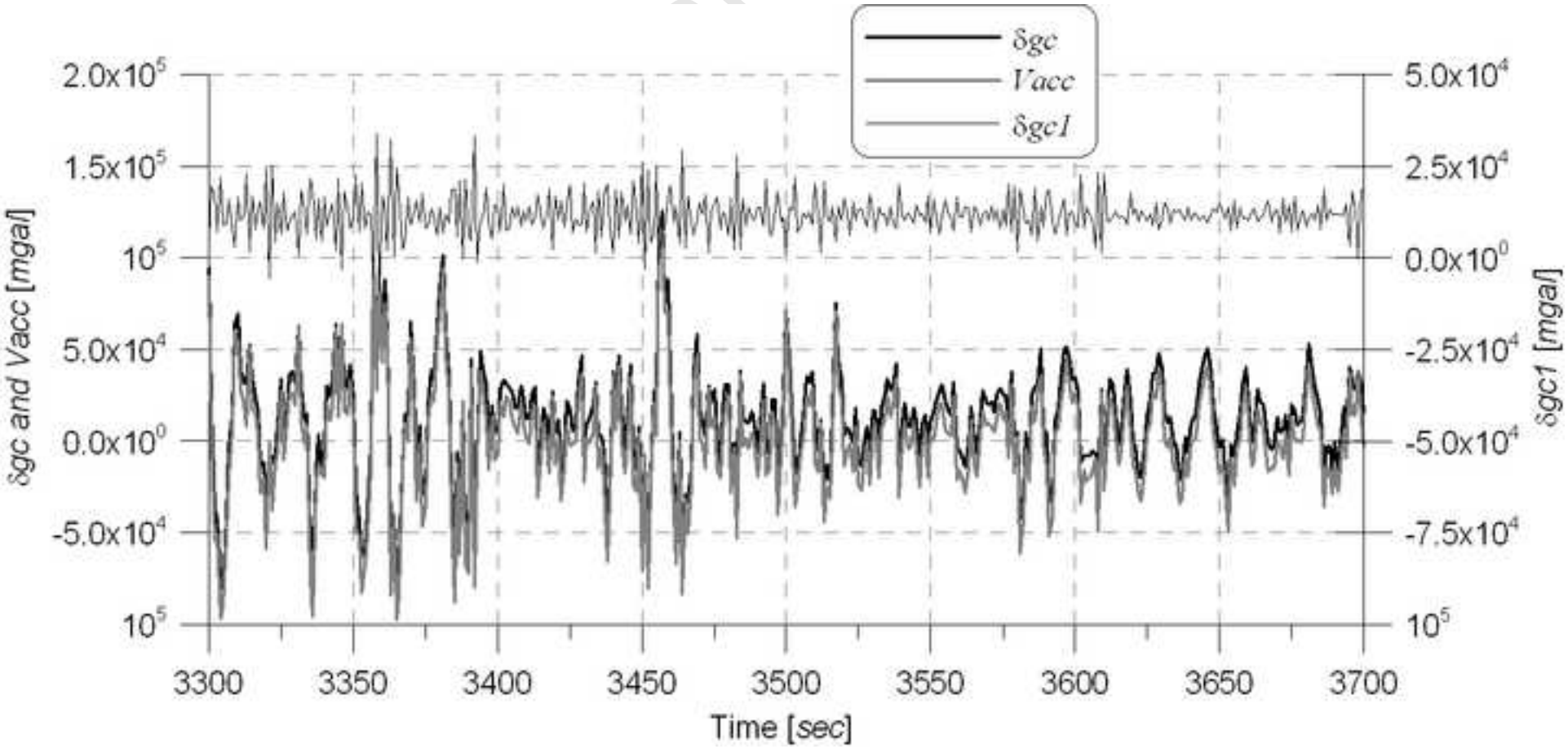
δgc
Vacc
δgc1
2.0x10^5
1.5x10^5
10^5
5.0x10^4
0.0x10^0
-5.0x10^4
10^5
5.0x10^4
2.5x10^4
0.0x10^0
-2.5x10^4
-5.0x10^4
-7.5x10^4
10^5
δgc and Vacc [mgal]
δgc1 [mgal]
3300
3350
3400
3450
3500
3550
3600
3650
3700
Time [sec]

Table 1 Properties of the IMU-IIb

	Gyroscopes	**Accelerometers**
Drift/Bias	0.3°/h	0.5 mg
Noise	0.05°/sqrt(h)	10 mg

Table 2 Accuracy observed minus modelled gravity anomalies

Model	no. of points	units	average	RMS	Minimum	Maximum
Slintax-*T*	1791	m^2/s^2	-0.0	0.6	-3.4	3.7
Slintax-δg_r	3326	mgal	0.0	0.8	-5.2	7.3